

A calibration-independent laser-induced incandescence technique for soot measurement by detecting absolute light intensity

David R. Snelling, Gregory J. Smallwood, Fengshan Liu, Ömer L. Gülder, and William D. Bachalo

Laser-induced incandescence (LII) has proved to be a useful diagnostic tool for spatially and temporally resolved measurement of particulate (soot) volume fraction and primary particle size in a wide range of applications, such as steady flames, flickering flames, and Diesel engine exhausts. We present a novel LII technique for the determination of soot volume fraction by measuring the absolute incandescence intensity, avoiding the need for *ex situ* calibration that typically uses a source of particles with known soot volume fraction. The technique developed in this study further extends the capabilities of existing LII for making practical quantitative measurements of soot. The spectral sensitivity of the detection system is determined by calibrating with an extended source of known radiance, and this sensitivity is then used to interpret the measured LII signals. Although it requires knowledge of the soot temperature, either from a numerical model of soot particle heating or experimentally determined by detecting LII signals at two different wavelengths, this technique offers a calibration-independent procedure for measuring soot volume fraction. Application of this technique to soot concentration measurements is demonstrated in a laminar diffusion flame. © 2005 Optical Society of America

OCIS codes: 120.1740, 010.1120.

1. Introduction

Recent studies have drawn attention to the role of combustion-generated particulate matter in global and regional climate change. Epidemiological studies also indicated that exposure to elevated levels of particulate matter exacerbates several pulmonary diseases, including asthma, bronchitis, and viral infections. The soot emitted from various combustion devices, such as engines, power generation facilities, incinerators, and furnaces, therefore not only represents a loss of useful energy but also is a serious environmental pollutant and a health risk. To assist

policy markers in regulating particulate emission, to develop techniques for controlling the emission of soot, and to assess its climate impact and health risk, we must first possess suitable means for reliably measuring various parameters, such as soot concentration and particle size. These methods must have an adequate dynamic range, be able to monitor and characterize the pollutant emissions over a very wide range of concentrations, and must operate under a range of environmental conditions from *in situ* exhaust to atmospheric monitoring. In the case of particulate matter, information on the particle mass, size distribution, and volume fraction is needed. The lack of suitable diagnostic tools has resulted in some uncertainty in the correlation of the particulate loading with health effects. A need for reliable techniques for measuring soot aerosol concentration in the atmosphere has been further demonstrated by recent studies showing that soot aerosol (black carbon) may be the second most important factor of global warming after carbon dioxide.^{1,2} Improvements in the instrumentation for soot diagnostics are urgently needed to help develop test protocols, standards, and regulations that will preserve the environment and reduce risks to human health.

Laser-induced incandescence (LII) measurement is

D. R. Snelling (dave.snelling@nrc.ca), G. J. Smallwood (greg.smallwood@nrc.ca), and F. Liu (fengshan.liu@nrc.ca) are with The Institute for Chemical Process and Environmental Technology, National Research Council Canada, Building M-9, 1200 Montreal Road, Ottawa, Ontario K1A 0R6, Canada. Ö. L. Gülder (ogulder@utias.utoronto.ca) is with the University of Toronto, Institute for Aerospace Studies, 4925 Dufferin Street, Toronto, Ontario M3H 5T6, Canada. W. D. Bachalo (wbachalo@aol.com) is with Artium Technologies, 14660 Saltamontes Way, Los Altos Hills, California 94022-2036.

Received 5 May 2005; accepted 8 June 2005.

0003-6935/05/316773-13\$15.00/0

© 2005 Optical Society of America

an emerging technology that promises to be a reliable means for spatially and temporally measuring the soot volume fraction and primary soot particle size. Eckbreth³ recognized the concept while working with Raman spectroscopy in flames and was troubled by the presence of soot particles that produced laser-modulated incandescence, which could overwhelm the desired Raman signals. He was able to relate the time dependence of this interference to laser particulate heating, heat transfer to the medium, particle vaporization, and indirectly to the particle size. Melton⁴ performed numerical calculations to investigate the possibility of developing a soot diagnostic based on this laser heating of particles. He concluded that the radiant emission from heated soot particles is proportional to soot concentration. Dasch⁵ modeled the vaporization of small soot particles and conducted experiments demonstrating the method.

In LII the soot within the path of a pulsed laser beam is heated rapidly from the local gas temperature to somewhere around the soot sublimation temperature (approximately 4000–4500 K) by using a pulsed laser source with a duration typically less than 20 ns (FWHM). The incandescence from the soot particles is measured by using collection optics and photodetectors. Using appropriate calibration and analysis of the incandescence signal, information on the soot volume fraction may be obtained. A number of research teams^{6–12} have investigated LII for quantitative soot concentration measurements by multiplying the LII intensity by a calibration factor C , i.e. $f_v = C \times I_p$. In these studies, the calibration factor C is obtained by correlating the LII intensity I_p to a known soot volume fraction f_v , which is either measured independently, such as by light attenuation or gravimetric sampling, or simply known because a well-controlled carbon black generator or another known source is used. In these conventional applications of LII for soot measurement, the laser fluence should be sufficiently high to be in the plateau region^{6,10,11} (soot particles are heated to 4000–4500 K to induce significant sublimation), where the LII signal intensity remains relatively independent of the laser pulse energy. For this conventional LII method, as long as there are no significant changes between the conditions of calibration and the LII measurements, the measured volume concentration should be relatively accurate. However, all particulates are not created equal. Calibrating in a flame at high temperature and then measuring at lower temperatures can introduce inaccuracies due to different peak temperatures. Furthermore, variation in the ambient pressure can also have an effect, as it affects the sublimation temperature of elemental carbon. Even calibration in engine exhaust will result in errors, as the composition of the particulates can change as the engine conditions change, again resulting in different peak temperatures. Because of these limitations of the conventional LII method, caution must be taken when applying the calibration constant obtained under a condition substantially different from the actual measurement condition in terms

of the local gas temperature, the chemical compositions of the particulate matter, and the ambient pressure. Nevertheless, LII can meet the need for soot particulate measurements, since the LII signal is proportional to the particulate volume fraction over a wide dynamic range.^{10,13–21} The LII technique is essentially nonintrusive and is capable of making *in situ* measurements over a very large range of soot concentrations in flames and ambient conditions. When operated in the sublimation regime (soot particle temperatures greater than about 3400 K), however, it is not completely nonperturbing, as the rapid laser heating can be expected to affect the soot morphology²² and cause some loss of carbon through sublimation during the short duty cycle of the laser.

In this paper we present a novel LII technique for quantitative soot volume fraction measurement by detection of the absolute LII intensity. This new LII technique relies on a detailed understanding of the nanoscale heat and mass transfer in time and space, which are commonly described by the mass and energy balance of an isolated single primary soot particle. The distinct advantage of this technique is that it does not need to be calibrated by using a source of soot particulates with a known concentration, and thus it extends the capabilities of LII for making practical quantitative soot measurements. The theoretical basis of this technique is first described below followed by its application to an atmospheric laminar diffusion flame.

2. Methodology

The fundamental idea behind the present LII technique is that the soot volume fraction can be determined if the absolute spectral intensity of the incandescence signal emitted from the laser heated soot particles is measured and the temperature of the soot particles is known. In order to measure the absolute LII intensity, the detection system must be calibrated by using a radiation source of known radiance. The soot particle temperature is required for calculating the theoretical spectral emission intensity per unit volume of soot. The temperature of soot particles can either be measured by detecting the LII signals at two different wavelengths, typically in the visible, or calculated numerically by solving a LII model simulating the soot particle heating and subsequent cooling processes. The calibration of the detection system and the theory for the determination of soot volume fraction by using the absolute LII intensity are discussed below.

In this study, the detection system is calibrated by using a strip filament lamp of known brightness temperature and thus known radiance. The calibration may also be performed with other sources, such as a source of known irradiance incident on a diffuser of known scattering efficiency and angular distribution. The optical setup for absolute light intensity calibration is shown schematically in Fig. 1. A calibrated strip filament lamp is located coincident with the location where LII signal is generated (i.e., where the soot concentration is to be measured). The filament is

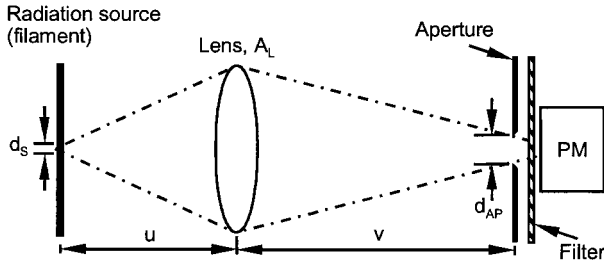


Fig. 1. Schematic of the optical setup for the calibration of absolute light intensity.

imaged with a lens of magnification M onto a circular aperture located in front of the photomultiplier. The lens magnification M is related to the distances u (between the radiation source and the lens) and v (between the lens and the aperture) as $M = u/v$. Similarly, the diameter or height of the radiation source to be viewed by the detection system d_s is equal to Md_{AP} , where d_{AP} is the diameter of the aperture. The cross-sectional area of the lens is A_L .

A. Calibrated Lamp Signal

The spectral radiance of the lamp (the power emitted per unit area, per unit solid angle, and per unit wavelength interval) is given by

$$R_S(\lambda, T) = \frac{2c^2 h \varepsilon(\lambda, T)}{\lambda^5} \left[\exp\left(\frac{hc}{k\lambda T}\right) - 1 \right]^{-1}, \quad (1)$$

where $\varepsilon(\lambda, T)$ is the filament emissivity as a function of wavelength λ and temperature T , c is the speed of light, h the Planck constant, and k the Boltzmann constant. The calibrated lamp has a known brightness temperature T_B (temperature at which a perfect black body would emit the same amount of radiation) at a wavelength of 649 nm from which the true filament temperature (T_{FIL}) can then be obtained as

$$T_{FIL} = \left\{ \frac{1}{T_B} + \frac{\lambda k}{h c} \ln[\varepsilon(\lambda, T_{FIL})] \right\}^{-1}. \quad (2)$$

In the derivation of Eq. (2) the Wien approximation was used, since $\exp(hc/k\lambda T)$ is much larger than 1 for the temperatures and wavelengths considered here ($1700 \text{ K} < T_B < 2000 \text{ K}$, $380 \text{ nm} < \lambda < 850 \text{ nm}$). The brightness temperature of the filament lamp is calibrated as a function of lamp current against a secondary standard photoelectric pyrometer at 649 nm. The uncertainty in the spectral radiance temperature of the strip filament lamp is $\pm 5 \text{ K}$. The variation in emissivity of tungsten with wavelength is taken from Pon and Hessler.²³

With the known emissivity of tungsten as a function of temperature and wavelength the filament radiance can be obtained at any desired wavelength from Eq. (1). The filament spectral radiant power incident on the aperture is given by

$$P_{CAL} = M^2 A_{AP} \frac{A_L}{u^2} R_S(\lambda, T_{FIL}), \quad (3)$$

where A_{AP} is the area of the aperture (i.e., $A_{AP} = \pi d_{AP}^2/4$) and A_L/u^2 is the collection solid angle of the lens. The observed voltage signal on the photomultiplier, V_{CAL} , from the calibration lamp then provides a detection system calibration and is given by

$$V_{CAL} = G_{CAL} Z M^2 A_{AP} \frac{A_L}{u^2} \int_{\lambda} R_S(\lambda, T_{FIL}) \times \Theta(\lambda) \tau(\lambda) d\lambda, \quad (4)$$

where $\Theta(\lambda)$ is the primary (photocathode) detector response in amperes per watt, G_{CAL} is the detector (photomultiplier) gain used in the calibration, $\tau(\lambda)$ is the filter transmission as a function of wavelength, and Z is the impedance of the measuring device.

B. LI Signal Intensity from Particulates

The total (over 4π sr) power radiated at wavelength λ by a single particle of diameter d_p , smaller than the wavelength of light, i.e. the particle is in the Rayleigh limit with $\pi d_p/\lambda < 0.3$, at temperature T_p is given by

$$P_p(\lambda, T_p) = \frac{8\pi^3 c^2 h}{\lambda^6} \left[\exp\left(\frac{hc}{k\lambda T_p}\right) - 1 \right]^{-1} d_p^3 E(m_\lambda) \\ = \frac{48\pi^2 c^2 h}{\lambda^6} \left[\exp\left(\frac{hc}{k\lambda T_p}\right) - 1 \right]^{-1} v_p E(m_\lambda), \quad (5)$$

where $E(m_\lambda)$ is a function of the soot refractive index and is called the soot absorption function, and $v_p = \pi d_p^3/6$ is the volume of the particle. Equation (5) can also be recast into the following form:

$$\Phi_p(\lambda, T_p) = \frac{P_p(\lambda, T_p)}{v_p} \\ = \frac{48\pi^2 c^2 h}{\lambda^6} \left[\exp\left(\frac{hc}{k\lambda T_p}\right) - 1 \right]^{-1} E(m_\lambda), \quad (5a)$$

which represents the total radiated power per unit volume of particulate. For typical combustion-generated soot particles, which are aggregates of relatively monodisperse spherical primary particles, Rayleigh–Debye–Gans (RDG) theory^{24,25} predicts that the absorption cross section of a soot aggregate is the sum of the absorption cross section of the constituent primary particles. More accurate numerical simulation has confirmed that this is a good approximation.^{26–30} For a particle (soot) volume fraction f_v the theoretical total power that would be observed experimentally is the power radiated by the total volume of particulate in the region of space that is imaged onto the detector. This volume is a cylinder of cross-sectional area $M^2 A_{AP}$ with a length defined by

the laser sheet thickness w_b for our configuration of sheet illumination and circular detection aperture. Assuming that the laser fluence is uniform in the laser beam (a more general case of nonuniform fluence profile across the laser sheet is discussed later), all the soot particles in the laser probe volume have the same initial temperature T_p (at the end of and shortly after the laser pulse) and the measured spectral power, P_{EXP} , is given by

$$P_{\text{EXP}} = \phi_p(\lambda, T_p) f_v M^2 A_{\text{AP}} w_b \frac{A_L}{4\pi u^2}. \quad (6)$$

This spectral power, P_{EXP} , will produce an experimental voltage signal V_{EXP} expressed as

$$V_{\text{EXP}} = Z G_{\text{EXP}} f_v M^2 A_{\text{AP}} \frac{A_L}{4\pi u^2} w_b \int_{\lambda} \phi_p(\lambda, T_p) \times \Theta(\lambda) \tau(\lambda) d\lambda, \quad (7)$$

where G_{EXP} is the detector gain used in the experiment. It is evident from a comparison of Eqs. (4) and (7) that the magnification (M), the aperture size (A_{AP}), and the collection solid angle of the lens (A_L/u^2) are common in both expressions. Thus the calibration and the expected LII signal depend on their magnitude in the same way. The integration over the filter bandwidth is also common to Eqs. (4) and (7) and largely cancels, as we shall see in the following sections. Thus, the strip filament calibration lamp provides a source of known radiance that we can compare with the particle (soot) radiation, largely independent of any exact knowledge of the filter characteristics, collection solid angle, or viewing region cross-sectional area.

C. Spectral Dependence of Light Attenuation

The integrals over the filter transmission bandwidth in Eqs. (4) and (7) are a function of the filter transmission, the radiance signal, and the detector sensitivity, since all these quantities can vary with wavelength. However, in practice, to a good approximation, we may replace these integrals with an equivalent filter with a center wavelength λ_C , a bandwidth Δ_{λ_C} , and a response $\tau(\lambda_C)\Theta(\lambda_C)$, where the bandwidth is defined as

$$\Delta_{\lambda_C} = \frac{\int_{\lambda} \tau(\lambda)\Theta(\lambda) d\lambda}{\tau(\lambda_C)\Theta(\lambda_C)} = \frac{\int_{\lambda} \tau(\lambda)\Theta(\lambda) d\lambda}{\Omega(\lambda_C)}, \quad (8)$$

where $\Omega(\lambda_C)$ represents $\tau(\lambda_C)\Theta(\lambda_C)$ and the integration is over the total filter bandwidth. The center wavelength, λ_C , is defined such that $\int_{\lambda_C}^{\lambda_C} \tau(\lambda)\Theta(\lambda) d\lambda = \int_{\lambda_C}^{\lambda_C} \tau(\lambda)\Theta(\lambda) d\lambda$. The integral in Eq. (4) can now be approximately replaced by $\Omega(\lambda_C)\Delta_{\lambda_C} R_S(\lambda_C, T)$, where we have approximated the lamp spectral radiance by its value at λ_C . Similar expressions can be used for

other integrals where we replace spectral quantities by the appropriate center line values. We have assessed the error associated with this equivalent filter approximation by comparing the results with those of the full integral expression. The largest error encountered (10%) was for a filter with a bandwidth of 40 nm, centred at 400 nm, a filament temperature of 1600 K, and a detector with a bi-alkali photocathode. This is the maximum error likely to be encountered, since the error decreases as the lamp (or particle) temperature and the center wavelength increase. At typical laser heated particle (soot) temperatures (2800–4000 K), the errors are expected to be less than 1%. A lamp-current-dependent correction factor was derived for the lamp calibrations. This correction factor is derived by calculating the ratio of the exact integral in Eq. (4) to the equivalent filter approximation in Eq. (4a) below. The calibration, based on the equivalent filter approximation, is then multiplied by this ratio. The calibration was always performed at three or more lamp currents, and the agreement between these calibrations was an indication that the resulting errors are negligible.

D. Soot Volume Fraction from an Absolute LII Signal

With the equivalent filter approximation, Eq. (4) can now be written as

$$V_{\text{CAL}} = G_{\text{CAL}} Z M^2 A_{\text{AP}} \frac{A_L}{u^2} R_S(\lambda_C, T_{\text{FIL}}) \Omega(\lambda) \Delta_{\lambda_C}. \quad (4a)$$

Equation (4a) can be rearranged to define a calibration factor η ;

$$\eta = \frac{V_{\text{CAL}}}{R_S(\lambda_C, T_{\text{FIL}}) G_{\text{CAL}}} = Z M^2 A_{\text{AP}} \frac{A_L}{u^2} \Omega(\lambda) \Delta_{\lambda_C}. \quad (4b)$$

With this calibration factor, Eq. (7) can now be expressed as

$$\frac{V_{\text{EXP}}}{\eta} = G_{\text{EXP}} f_v w_b \frac{1}{4\pi} \phi_p(\lambda_C, T_p). \quad (7a)$$

From Eq. (7a) the soot volume fraction f_v is obtained as

$$f_v = \frac{V_{\text{EXP}}}{\eta w_b G_{\text{EXP}} \frac{12\pi c^2 h}{\lambda_C^6} E(m_{\lambda_C}) \left[\exp\left(\frac{hc}{k\lambda_C T_p}\right) - 1 \right]^{-1}}. \quad (9)$$

It is noted that the polydispersity of primary soot particle diameters, which causes nonuniformity in particle temperatures after the laser pulse owing to the slower cooling rate of larger particles, is not considered in the present development because the dis-

tribution of primary soot particle diameters³¹ at a given location in flames is relatively narrow. All the quantities on the right-hand side of Eq. (9) are known with the exception of the soot particle temperature T_p .

E. Particulate Temperature

To determine the soot concentration by using Eq. (9) it is necessary to know the soot temperature. We first discuss the temperature of soot particles heated by a laser with spatially uniform fluence. In this case, all the soot particles in the laser probe are heated uniformly and have the same temperature, as mentioned earlier. The soot particle temperature can be derived from the principle of two-color optical pyrometry by detecting the particle incandescence signals at two wavelengths in the visible. From Eq. (5) and using the Wien approximation, $\exp[hc/(k\lambda_c T_p)] \gg 1$, we can derive an expression for the ratio of soot particle incandescence intensities at wavelengths λ_1 and λ_2 . The error involved in adopting the Wien approximation increases with increasing temperature and wavelength. As an example, the Wien approximation underpredicts the radiation intensity by 1.7% for $T_p = 4500$ K and $\lambda = 780$ nm. The error is even smaller for lower temperatures and wavelengths and is in general negligible for conditions normally encountered in LII. From Eq. (5) and using the Wien approximation, one can obtain the following expression:

$$\frac{P_p(\lambda_1)}{P_p(\lambda_2)} = \frac{\lambda_2^6 E(m_{\lambda_1})}{\lambda_1^6 E(m_{\lambda_2})} \exp\left[-\frac{hc}{kT_p} \left(\frac{1}{\lambda_1} - \frac{1}{\lambda_2}\right)\right]. \quad (10)$$

The ratio of the incandescence intensities at λ_1 and λ_2 can be related to that observed experimentally by making use of Eq. (7a):

$$\frac{\lambda_2^6 E(m_{\lambda_1})}{\lambda_1^6 E(m_{\lambda_2})} \exp\left[-\frac{hc}{kT_p} \left(\frac{1}{\lambda_1} - \frac{1}{\lambda_2}\right)\right] = \frac{V_{\text{EXP1}} \eta_2 G_{\text{EXP2}}}{V_{\text{EXP2}} \eta_1 G_{\text{EXP1}}}. \quad (11)$$

The particle temperature T_p can therefore be derived from this expression, since all other values in Eq. (11) are known. To eliminate the error in the particle temperature calculated from Eq. (11), due to use of the Wien approximation, the efficient iteration method suggested by Levendis *et al.*³² can be followed, which finds the true particle temperature in just one or two iterations. Once T_p is obtained, it can be substituted into Eq. (9) to calculate the soot volume fraction.

In general, however, the laser fluence profile across the laser sheet is not uniform. In this case, soot particles in different parts of the laser sheet are subject to different laser fluences and therefore have different temperatures. The detected LII signal is then the total contribution from all the soot particles of different temperatures within the laser volume. Here we assume that the only variation in fluence occurs

along the viewing axis x , i.e., across the laser sheet. By further assuming that soot particles are uniformly distributed inside the laser probe volume, i.e., that there is no variation in soot volume fraction, and that the laser probe volume is small enough to ensure the validity of the optically thin approximation, we can relate the experimental voltage signal V_{EXP} to the soot particle temperature distribution across the laser sheet as, based on Eq. (7a),

$$\frac{V_{\text{EXP}}}{\eta} = G_{\text{EXP}} f_v \frac{12\pi c^2 h}{\lambda_c^6} E(m_{\lambda_c}) \int_x \left\{ \exp\left[\frac{hc}{k\lambda_c T_p(x)}\right] - 1 \right\}^{-1} dx. \quad (7b)$$

It should be pointed out that in deriving Eq. (7b) from Eq. (7a) it is implicitly assumed that the peak laser fluence is sufficiently low to ensure negligible sublimation of soot mass; otherwise, the particle size d_p will also vary with location x in the laser sheet, just like the particle temperature T_p . In addition, it is preferred to operate LII in the nonsublimation regime, where the peak particle temperature³³ remains below about 3400 K, since the absence of soot mass loss makes the measurements truly nonintrusive.

F. Equivalent Laser Sheet Thickness

For a nonuniform spatial fluence profile, as expressed in Eq. (7b), the experimental voltage signal V_{EXP} is related to the total incandescence signal contributed by soot particles of different temperatures across the laser sheet. Even so Eq. (11) can still be used to define an effective temperature T_{pe} based on the ratio of the two experimental voltage signals V_{EXP1} and V_{EXP2} . However, the effective temperature obtained from Eq. (11) now represents some average temperature heavily biased toward the highest particle temperature in the laser probe volume, since the incandescence signal is exponentially dependent on temperature. This effective temperature cannot be directly used in Eq. (9) for the determinant of soot volume fraction, since the laser sheet thickness w_b is no longer a well-defined parameter when the fluence across the laser sheet is nonuniform, such as in a Gaussian profile. However, by using T_{pe} , as calculated from Eq. (11), an equivalent laser sheet thickness w_e can be defined as such that

$$w_e \left[\exp\left(\frac{hc}{k\lambda_c T_{pe}}\right) - 1 \right]^{-1} = \int_x \left\{ \exp\left(\frac{hc}{k\lambda_c T_p(x)}\right) - 1 \right\}^{-1} dx, \quad (12)$$

and from this, the soot volume fraction is now expressed as

$$f_v = \frac{V_{\text{EXP}}}{\eta G_{\text{EXP}} \frac{12\pi c^2 h}{\lambda_c^6} E(m_{\lambda_c}) w_e \left[\exp\left[\frac{hc}{k\lambda_c T_{pe}}\right] - 1 \right]^{-1}} \quad (9a)$$

To calculate the equivalent laser sheet thickness and ultimately solve for the soot volume fraction using by Eq. (9a) for the general case of nonuniform laser fluence, we must rely on numerical calculations to supplement the experimental analysis. In this numerical approach, a series of numerical calculations are first performed by using a LII model^{19,34,35} for a range of fluence values. These calculations set up a database in which the history of soot particle temperature and diameter at prescribed values of laser fluence are stored. With the help of this database, the integral on right-hand side of Eq. (12) can be numerically evaluated for any experimentally obtained fluence distribution $F(x)$ across the laser sheet, as long as the prescribed fluence values in the database cover the entire range of $F(x)$. The particle temperature, $T_p(x)$, at any given location x_i in the laser sheet, corresponding to a laser fluence of $F(x_i)$, is calculated by a simple linear interpolation between the solutions of its two neighboring values of laser fluence in the database. The effective particle temperature T_{pe} on the left-hand side of Eq. (12) can be evaluated either experimentally from Eq. (11) or theoretically. In the latter case, the effective temperature is found by solving the following equation:

$$\frac{\lambda_2^6 E(m_{\lambda_1}) \int_x \left\{ \exp\left[\frac{hc}{k\lambda_1 T_p(x)}\right] - 1 \right\}^{-1} dx}{\lambda_1^6 E(m_{\lambda_2}) \int_x \left\{ \exp\left[\frac{hc}{k\lambda_2 T_p(x)}\right] - 1 \right\}^{-1} dx} = \frac{\lambda_2^6 E(m_{\lambda_1})}{\lambda_1^6 E(m_{\lambda_2})} \exp\left[-\frac{hc}{kT_{pe}} \left(\frac{1}{\lambda_1} - \frac{1}{\lambda_2}\right)\right]. \quad (13)$$

In doing so, we are actually numerically simulating the ratio of the detected incandescence signals at λ_1 and λ_2 . It should be pointed out that although this theoretical effective temperature is independent of the values of $E(m)$ at the two detection wavelengths—they appear on both sides of Eq. (13) and therefore cancel out—it is strongly dependent on the value of $E(m)$ at the laser wavelength. Because of the known uncertainty in the value of $E(m)$, the calculated effective particle temperature is also subject to uncertainty caused by (i) uncertainty in $E(m)$ at the laser wavelength, and (ii) error in the experimental laser pulse energy (fluence). A small error in the particle effective temperature gives rise to a large error in the derived soot volume fraction. Therefore this theoretical approach for the determination of the effective particle temperature is in general not recommended.

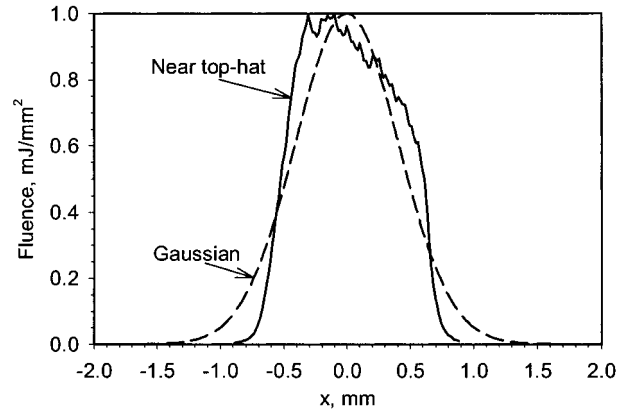


Fig. 2. Two nonuniform laser fluence profiles assumed in the evaluation of the equivalent laser sheet thickness. The Gaussian profile is generated with $F(x) = F_{\text{max}} \exp(-x^2/2\sigma^2)$, $\sigma = 0.41$, and $F_{\text{max}} = 1 \text{ mJ/mm}^2$. The two laser fluence profiles cover the same area.

However, the numerically calculated equivalent laser sheet thickness is quite insensitive to the laser pulse energy or the value of $E(m)$ shown below. Finally, the equivalent laser sheet thickness w_e can be calculated from Eq. (12). This numerically derived equivalent thickness is potentially a function of the laser fluence profile, the peak fluence value, time, and particle size.

In practice we hope that the equivalent laser sheet thickness does not vary significantly with time, particle size, or the peak laser fluence. Otherwise, it is difficult to use this quantity in the evaluation of the soot volume fraction by using Eq. (9a). To demonstrate how w_e varies with time, peak laser fluence, and particle size for a known shape of laser profile, numerical calculations were conducted by using the LII model described previously.^{34,35} The temporal profile of the laser was assumed to be same as that shown in Ref. 36. In the calculation, the gas temperature is $T_g = 1700 \text{ K}$, the laser wavelength is 1064 nm , and the soot absorption function at 1064 nm and the soot thermal accommodation coefficient are, respectively, 0.4 and 0.37 based on our previous study.³⁶ Two spatial laser fluence profiles are investigated: one is a near top-hat and the other one is a Gaussian profile, as shown in Fig. 2 for a peak fluence value of 1 mJ/mm^2 . The two curves were normalized to represent the same laser energy (same spatially integrated fluence profile). It is noted that these two lasers have the same temporal profile shown in Ref. 36. Figure 3 displays the variation of w_e with time for three soot particle diameters and two peak laser fluence values. The range of particle diameter investigated, from 15 to 45 nm , covers almost the entire primary particle diameter distribution in flame-generated soot. Larger values of the peak laser fluence were not calculated, since even at $F_{\text{max}} = 1.25 \text{ mJ/mm}^2$ the peak effective soot particle temperature in both laser profiles reaches about 3600 K and results in nonnegligible soot sublimation. In the case of a lower peak laser fluence, $F_{\text{max}} = 1.0 \text{ mJ/mm}^2$, the peak effective particle temperature

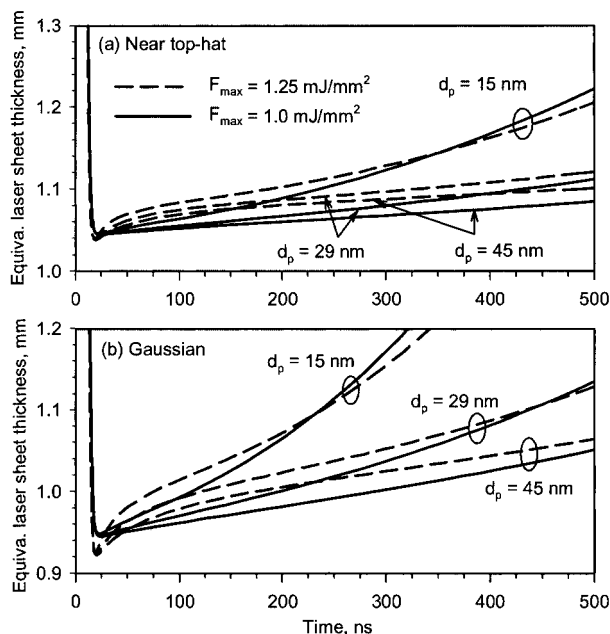


Fig. 3. Variation of the equivalent laser sheet thickness with time for three primary soot particle diameters and two peak values of laser fluence.

is only around 3230 K; hence soot sublimation does not occur. The time at the lowest equivalent laser sheet thickness in Fig. 3 corresponds roughly to the end of the laser pulse. It can be seen that the equivalent laser sheet thickness first decays very rapidly from the entire physical width of the laser sheet shown in Fig. 2 to a minimum, then gradually increases. The initial rapid drop in w_e is associated with the rapid particle temperature rise due to laser energy absorption. The occurrence of a minimum w_e at the end of the laser pulse is an indication that the nonuniformity in particle temperatures across the laser sheet reaches its maximum. The subsequent rise in w_e implies a decrease in the particle temperature nonuniformity due to the cooling process, which eventually brings the particle temperatures back to the gas temperature. The somewhat more rapid increase in w_e after the laser pulse in the case of the higher peak laser fluence is associated with the reduction of particle diameter in the central part of the laser sheet due to sublimation. Even in this case, the equivalent laser sheet thickness increases only 11% from its minimum value at 100 ns after the laser pulse for the Gaussian profile and only 5% for the near top-hat profile. These variations are for the smallest particle diameter considered, i.e., $d_p = 15$ nm. For larger particle diameters, the variation of w_e within 100 ns after the laser pulse is even smaller. In the nonsublimation situation, i.e., $F_{\max} = 1.0$ mJ/mm², the largest variation of w_e from its minimum value at 100 ns after the laser pulse is only about 6.4%, which occurs for $d_p = 15$ nm and the Gaussian profile. Therefore it can be concluded that the equivalent laser sheet thickness in general increases less than 5% from its minimum value within

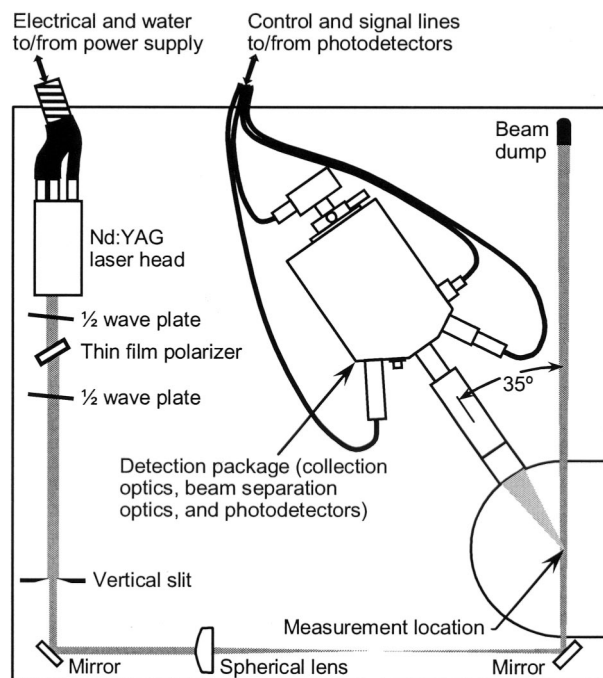


Fig. 4. Top-view schematic of the optical and detection apparatus used in the LII experiment.

100 ns after the laser pulse provided that the peak laser fluence is sufficiently low, i.e., that the peak particle temperatures are lower than about 3400 K to ensure negligible soot sublimation. It is also noted from Fig. 3 that the equivalent laser thickness is quite insensitive to the particle diameter and the peak laser fluence. The insensitivity to the peak laser fluence can be viewed as insensitive to both the value of $E(m)$ at the laser wavelength and the laser pulse energy, since the soot particle energy absorption rate is proportional to the product of $E(m)$ and laser fluence.³⁵ This is indeed a desired property, as the numerically calculated w_e is only subject to small uncertainty even when there are moderate uncertainties in the value of $E(m)$ or the laser pulse energy. The minimum value of w_e just after the laser pulse for the lower peak fluence curve is 0.95 mm, which is very close to (within 2%) the Gaussian FWHM (full width at half-maximum) of 0.966 mm.

3. Experimental Procedure

The experimental apparatus is shown schematically in Fig. 4. The laser is a frequency doubled Q-switched Nd:YAG with an output at 532 nm of 30 mJ and a pulse width of 6.6 ns FWHM. The laser energy is controlled by means of a half-wave plate and a thin-film polarizer. The final polarization direction is selected by a half-wave plate and is vertically polarized for all experiments.

A rectangular slit was inserted into the laser beam. This slit was imaged at the measurement location to avoid diffraction effects and to generate a 532 nm beam with a more uniform energy distribution across a rectangular profile 1.5 mm wide and 3 mm high at

the probe volume focal point. The LII radiation was focused into a 1.0 mm core fiber of 0.16 numeric aperture by a pair of 50.8 mm diameter achromats of 150 mm focal length. The lenses were operated at infinite conjugate and were apertured to 40 mm diameter.

In the receiver, the light exiting from the fiber tip was collimated with a 50 mm achromatic lens, forming a beam of approximately 20 mm diameter. The beam was split into separate wavelength components by means of beam splitters. Interference filters at 400 and 780 nm with bandwidths of 40 and 20 nm, respectively, were used to limit the radiation incident on photomultiplier tube detectors (PMs). Two different PMs were selected to maximize sensitivity for each of the wavelengths. Lenses after the interference filters form an image of diameter 4.5 mm at the photocathode surface. The signals from the two photomultipliers were digitized by using a digital oscilloscope. The rise time of the photomultiplier signal was estimated to be ~ 1.5 ns from a comparison of the temporal dependence of the laser pulse detected by the PM to that from a fast silicon photodiode.

The transmission curve for each arm of the receiver was calculated from the measured transmission/reflections curves of the individual optic components. This overall transmission was checked by using a calibrated irradiance standard lamp, a spectrometer, and an integrating sphere. The irradiance source was reflected off a Lambertian diffuser block of known efficiency to provide a secondary source of known radiance. The diffuser surface was imaged, by using the collection optics achromat pair, onto the fiber tip. The white light emitted from the fiber was injected into an integrating sphere, which was then input into the spectrometer. The spectrum recorded provided a measure of the incident intensity. The fiber was then installed in the receiver, and the light in each channel, normally incident on the photomultiplier, was injected into the integrating sphere. The ratio of the spectrum so recorded to the incident light spectrum (both corrected for any background signal) provides an independent measure of the transmission of each arm. With the known cathode response of the PM, this transmission curve was used to calculate a center wavelength and a filter equivalent width as described above. The two methods of assessing the transmission were in agreement and provided the same center wavelength and filter equivalent width to better than 5%.

The system calibration described above using a calibrated strip filament lamp was also checked by using an irradiance standard and calibrated diffuse reflector to provide a secondary radiance source. These two methods provided calibration factors [Eq. (4b)] that agreed with each other to within 5% or better.

The energy profile (in arbitrary units) of the 532 nm Nd:YAG laser beam was measured by using a beam analyzer. From the integrated energy profile and the known laser energy the beam profile was converted into a two-dimensional fluence map at the measurement location. The measurement volume is

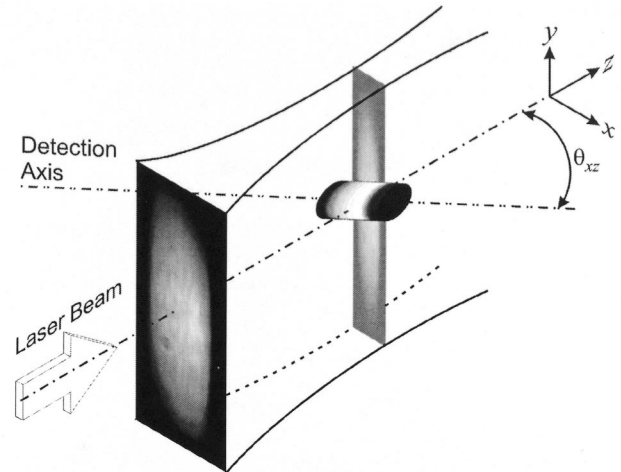


Fig. 5. Schematic of the coordinate system, illustrating the detection volume and the variation of the laser fluence in different directions.

defined by the cross sectional area of the image of the fiber tip at the sampled region and the laser sheet thickness. We can define a coordinate system where the laser propagation axis is z , the axis across the laser sheet is x , and the dimension corresponding to the sheet height is y . This coordinate system is schematically shown in Fig. 5. The angle between the laser beam and the viewing optic axis θ_{xz} was 35° . Thus the effective sheet thickness was $w_e/\sin(\theta_{xz})$. The fluence was essentially constant in the y direction of the laser sheet, since only the central portion of the sheet was viewed by the fiber. The intensity was therefore averaged along this axis (based on the viewed region), and the resulting average fluence as a function of distance x from the center of the sheet is shown in Fig. 6. The constancy of the fluence in the y

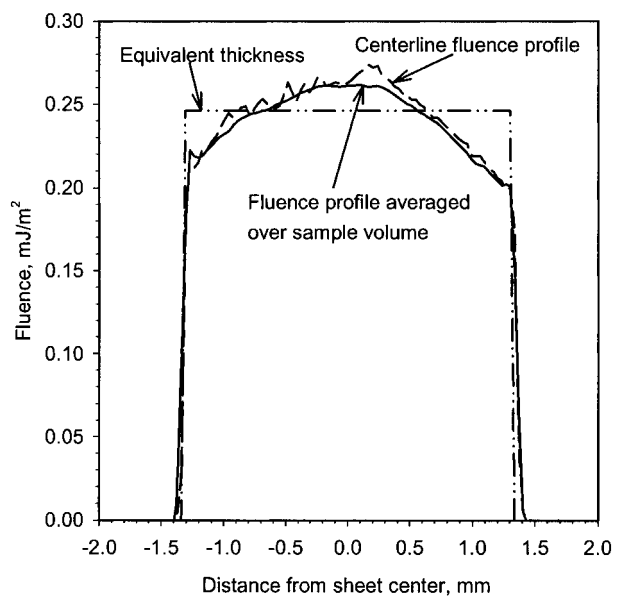


Fig. 6. Laser fluence profile along the detection axis in the sampled region.

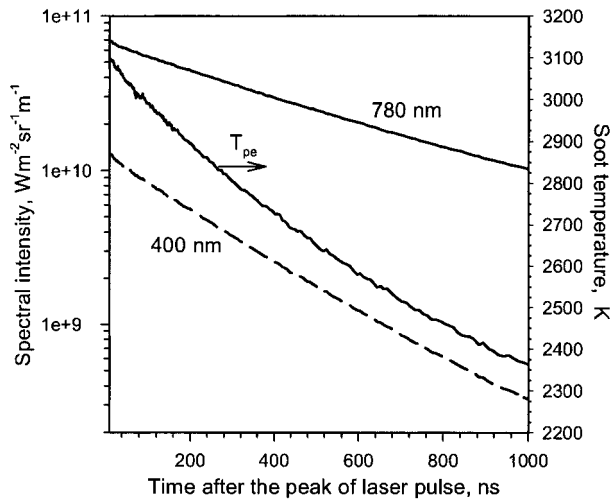


Fig. 7. Absolute LII signal intensities detected at 400 and 780 nm and the resultant soot temperature for a fluence of 0.376 mJ/mm^2 .

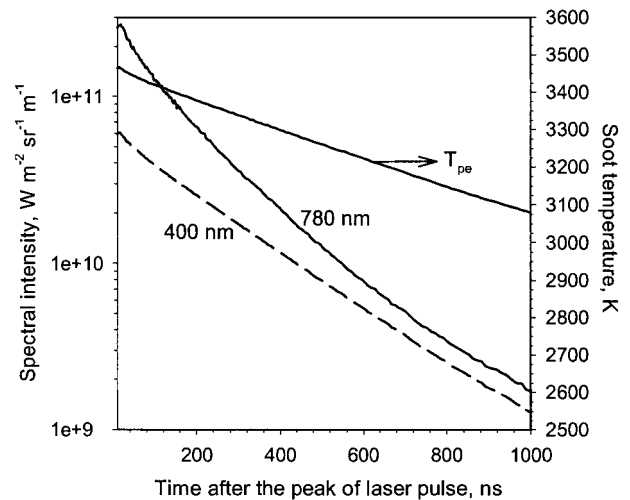


Fig. 8. Absolute LII signal intensities detected at 400 and 780 nm and the resultant soot temperature for a fluence of 0.502 mJ/mm^2 .

direction can be judged from the agreement of the y averaged fluence and the fluence profile through the center of the laser sheet. An equivalent sheet thickness was calculated from the average intensity over the center 90% of the laser sheet and a width that provide the same area as the spatially integrated fluence curve. As can be seen from Fig. 6, the fluence varies little across the laser sheet. In fact the equivalent thickness, calculated as described above, is within 5% of the thickness shown in Fig. 6, which was adopted in calculations discussed below. In addition, this thickness remains almost constant for a long time after the laser pulse owing to the absence of two wings in this fluence profile compared with those of the near top-hat and the Gaussian profiles shown in Fig. 3.

The burner for generating the laminar coflow ethylene diffusion flame at atmospheric pressure used in the present study was previously described in detail in Ref. 37. Briefly, the burner consists of a central fuel tube with a 10.9 mm inner diameter surrounded by an annular air nozzle of 100 mm inner diameter. The ethylene flow rate was $3.23 \text{ cm}^3/\text{s}$, and the air flow rate was $4733 \text{ cm}^3/\text{s}$, resulting in a visible flame height of about 64 mm. The present LII experiments were carried out at a location of 42 mm above the burner exit and on the burner centerline.

4. Results and Discussion

The temporal variation of LII intensities detected at the two wavelength bands and the resultant effective particle temperatures are shown in Figs. 7 and 8 for two different fluence values (mean value corresponding to the equivalent thickness), which were calculated from the equivalent thickness curve in Fig. 6. The absolute intensities were calculated as $V_{\text{EXP}}/\eta G_{\text{EXP}}$, and the resulting temperature from Eq. (11). A constant value³⁷ of $E(m)$ of 0.26 was assumed for both 400 and 780 nm in calculating the temperature. The absolute value of $E(m)$ affects only the

subsequent soot volume fraction and not the derived temperature, which depends only on the ratio of $E(m)$ at the two wavelengths. The time is expressed in nanoseconds after the peak of the laser pulse. The oscilloscope is triggered from the laser Q-switch sync out pulse, which has a time jitter of much less than 1 ns. The laser pulse can be seen on both channels if a diffuser is placed at the sample location to scatter the laser radiation. This provides a convenient method of establishing the time base for the two detection channels (400 and 780 nm) in relation to the laser pulse whose peak position is measured to better than 2 ns.

The soot volume fraction, calculated from Eq. (9) along with the experimental soot temperature shown in Figs. 7 and 8 and using an $E(m)$ of 0.26, is shown in Fig. 9. In spite of the difference in soot temperature for the two experiments shown in Figs. 7 and 8, the calculated soot volume fraction is essentially the same under conditions of the two different laser fluences. This is indeed the expected performance of the present LII technique: the difference in soot particle temperature caused by using different laser fluences is properly reflected in the difference in the absolute incandescence signal intensities. In fact, this same behavior is observed over a much wider range of soot temperatures (laser fluences). To demonstrate this we have also included in Fig. 9 the smoothed soot volume fraction for two additional fluence values of 0.251 and 0.151 mJ/mm^2 . The soot temperatures at 30 ns after the peak of the laser pulse were 2674 K (0.251 mJ/mm^2) and 2252 K (0.151 mJ/mm^2) for these two fluence values. The observed soot concentration immediately after the laser pulse is $3.8 \pm 0.1 \text{ ppm}$ (parts in 10^6) independent of laser fluence or soot temperature. At later times there is some small, but with a clear trend, variation in the derived soot volume fraction with time. From Fig. 9, it appears that there may be a small increase in soot volume fraction with time for

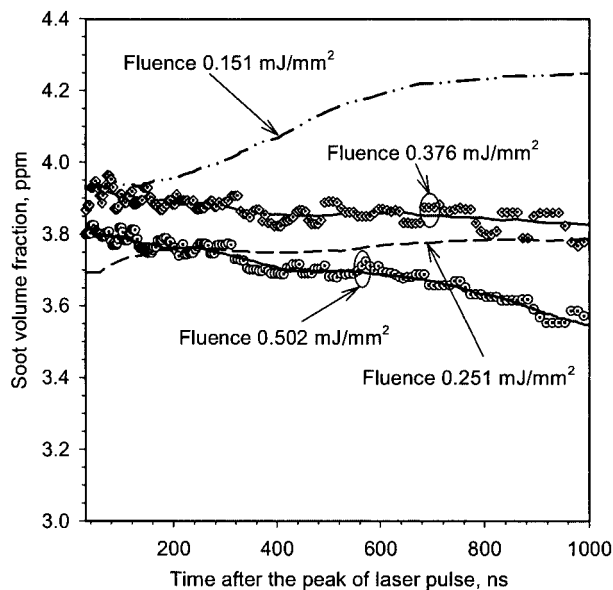


Fig. 9. Variation of the soot volume fraction measured using the present LII technique with time, at 42 mm above the burner exit and on the flame centerline for various values of laser fluence.

the lower fluence values and a slight decrease for the higher fluence values. It was initially thought that this is surprising, since there is essentially no soot sublimation at the particle temperatures of these experiments (there is some, but insignificant, soot sublimation at the highest fluence investigated, i.e., 0.502 mJ/mm^2) and that the calculated soot volume fraction should not vary with time. One potential factor that could cause the calculated soot volume fraction to vary with time is the use of a constant equivalent thickness of the laser sheet in the analysis. This is because the equivalent laser sheet thickness in general increases with time after the laser pulse as shown in Fig. 3, where the equivalent thickness increases significantly with time substantially after the laser pulse for the two laser fluence profiles illustrated in Fig. 2. As mentioned earlier, however, the equivalent thickness of the laser used in the experiments, Fig. 6, varies only slightly with time, and the use of a constant value in the analysis of the soot volume fraction is therefore justified and is not the reason for the variation of soot volume fraction with time shown in Fig. 9. A plausible explanation of the time dependence of the soot volume fraction lies in the shielding effect on the conduction heat loss of aggregated soot particles after the laser pulse. It is well known that in flames soot particles appear as mass fractal aggregates with a wide distribution in size (the number of primary particles) from one up to several hundreds or even thousands, rather than isolated single primary particles. The shielding effect refers to the fact that within an aggregate some primary particles are partially or even completely blocked by other primary particles from collision by the gas molecules. In other words, the shielding effect leads to a reduced surface area for heat transfer from soot aggregates to the surrounding gas. This effect

has been studied recently by Filippov *et al.*³⁸ and Liu *et al.*³⁹ Immediately after the laser pulse there is no variation in the LII signal (soot particle temperature) with aggregate size, since both the laser absorption and the subsequent emission from the hot soot are linearly dependent on the particle volume, and the laser energy absorption and the subsequent emission are not affected by aggregation based on the RDG theory mentioned earlier. However, soot particle aggregation affects the heat conduction rate through the shielding effect in such a way that larger aggregates cool slower than smaller ones.³⁹ As soot aggregates of different sizes have an almost identical temperature at the end of the laser pulse, the difference in the particle temperature of different aggregate sizes gradually increases at longer times. As a result, the experimental effective soot temperature is one that is averaged not only over the nonuniform laser profile but also over the temperature distributions among different aggregate sizes. Similarly to the shielding effect, the polydispersity of primary soot particle size (diameter) also causes temperature non-uniformity among primary soot particles as larger primary soot particles cool slower than smaller ones after the laser pulse. Accordingly, the particle temperature nonuniformity caused by the distributions of aggregate size and primary particle diameter should be accounted for in the evaluation of the equivalent laser sheet thickness. Since the objective of this paper is to present the methodology and demonstrate the principle and feasibility of this novel LII technique, the effects of the aggregate size distribution and primary particle diameter distribution on the equivalent laser sheet thickness and ultimately on the calculated soot volume fraction was not taken into account in the analysis.

The soot volume fraction at 42 mm on the burner centerline obtained by the present LII technique can be compared with that from light absorption measurements. As discussed above, the absorption of a soot aggregate is the sum of the total absorptions of its constituent primary particles, and thus the absorption measurement can be used to deduce the soot volume fraction provided that the soot absorption factor $E(m)$ is known. We have carried out two-dimensional light extinction measurements followed by Abel inversion of the line-of-sight transmission³⁷ to get the radial soot concentration profiles in the identical laminar diffusion flame. The extinction includes both absorption and scattering. If the ratio of light scattering to light absorption, ρ_{SA} , is known, the extinction-based soot volume fraction can be corrected by dividing it by $1 + \rho_{SA}$. Thermophoretic sampling of soot particles at the same location as the LII experiment and the subsequent TEM analysis⁴⁰ showed that the aggregate size distribution can be fitted to a lognormal function with a geometric mean N_g of 23 and a geometric standard deviation σ_g of 4. Angular scattering measurements at the same location in the flame were fitted to a lognormal function with an N_g of 18 and a σ_g of 2.6. These experimental lognormal distribution parameters were used to nu-

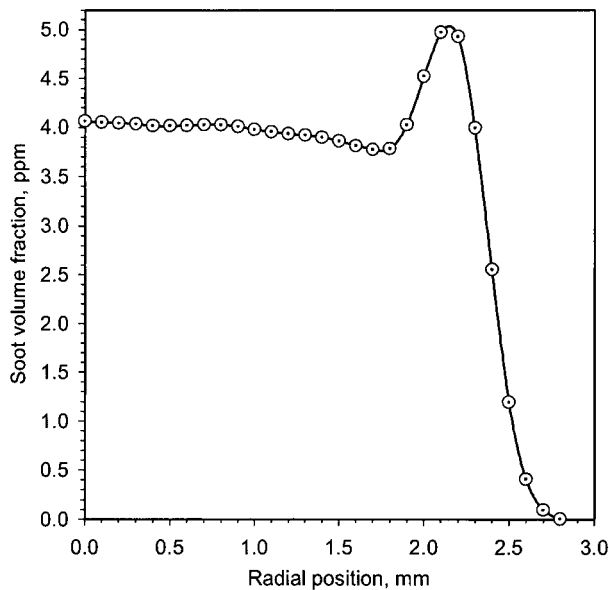


Fig. 10. Radial soot profile at 42 mm above the burner exit and on the flame centerline in the laminar diffusion flame from two-dimensional attenuation measurements at 577 nm.

merically calculate the ratio of scattering to absorption using the approach of Sorensen⁴¹ and a value of 1.0 for the ratio of the soot scattering function $F(m)$ to the absorption function $E(m)$ at 577 nm (Ref. 42), which was the wavelength used in the two-dimensional extinction measurements. For the experimental N_g and σ_g values mentioned above, the scattering to extinction ratio ρ_{SA} at 577 nm was found to be 0.097 ± 0.02 . The uncertainty in ρ_{SA} was due to the difference in the values of N_g and σ_g from the thermophoretic sampling with TEM and the scattering experiments. Therefore the factor used to correct the extinction-based soot volume fraction, $1 + \rho_{SA}$, is 1.097 ± 0.02 . The radial distribution of the soot volume fraction at 42 mm above the burner exit surface from the light extinction measurements is shown in Fig. 10. It is worth pointing out that the soot volume fraction shown in Fig. 10 was calculated by using the same $E(m)$ value of 0.26 assumed in the LII analysis. The sample length in the LII experiment was about ± 1.3 mm around the burner center. Figure 10 indicates that in the region sampled by LII the light absorption measurements give a soot volume fraction of 4.0 ± 0.1 ppm, which is in excellent agreement with the 3.8 ± 0.1 ppm from the present LII technique. Although the choice of 0.26 for $E(m)$ is somewhat uncertain, it affects the values of the soot volume fraction determined in both the LII and the light extinction measurements in the same way, and the value of $E(m)$ assumed should not alter the level of agreement in the soot volume fraction between these two techniques as long as the same value of $E(m)$ is used in analysis of both measurements. The agreement in the soot volume fraction from the LII and the light absorption techniques offers no evidence as to the appropriateness of 0.26 for the value

of $E(m)$ at 577 nm, since the soot volume fraction from both techniques is inversely proportional to the value of $E(m)$ assumed. The soot temperatures derived from LII signals and hence the resultant soot volume fraction are, of course, dependent on the assumed spectral variation of $E(m)$. As noted above we have assumed a constant $E(m)$ based on our earlier work,⁴³ which is consistent with the available data for $E(m)$ in the visible range summarized in Ref. 42. The agreement in soot volume fraction derived from LII and light absorption measurements, however, supports the assumption of constancy of $E(m)$ over the spectral region between 400 and 780 nm.

5. Conclusion

A novel LII technique was developed for measurement of the soot volume fraction in the nonsublimation regime. The technique relies on detecting the time-resolved absolute incandescence intensities at two wavelengths in the visible so that the effective soot temperature can also be determined. For an arbitrary fluence profile across the laser sheet, the analysis of the experimental data has to be complemented by using the concept of the equivalent laser sheet thickness. A numerical approach was developed to calculate the equivalent thickness based on the numerical solutions to a LII model at a series of prescribed values of laser fluence in the nonsublimation regime. Knowledge of the laser fluence profile is required in order to calculate the equivalent thickness. Because the time-resolved soot temperature is measured in this LII technique and the numerically calculated equivalent laser sheet thickness is in general not sensitive to the peak fluence as long as there is no significant soot sublimation, there is no need to know the exact value of the laser pulse energy used in the experiment. The distinct advantage of the present LII technique over the existing ones is that it does not need to be calibrated by using a source of soot of a known volume fraction. This novel technique further extends the capabilities of LII for quantitative measurement of the soot volume fraction. Application of the LII technique developed in this study was demonstrated in measuring the soot volume fraction in an atmospheric pressure coflow laminar ethylene diffusion flame. The soot volume fraction measured using this LII technique is in very good agreement with that from light extinction measurement, indicating that the LII technique is capable of making reliable measurement of the soot volume fraction.

The financial support from the Program of Energy Research and Development (PERD) is gratefully acknowledged. The authors also acknowledge the contributions of Kevin A. Thomson, who critically reviewed the manuscript and offered many valuable suggestions, and the technical support of Robert Sawchuk, Dan Clavel, and Daniel Gareau.

References

1. J. Hansen, M. Sato, R. Ruedy, A. Lacis, and V. Oinas, "Global Warming in the twenty-first century: an alternative scenario," *Proc. Nat. Acad. Sci.* **97**, 9875–9880 (2000).

2. M. Z. Jacobson, "Strong radiative heating due to the mixing state of black carbon in atmospheric aerosols," *Nature* **409**, 695–697 (2001).
3. A. C. Eckbreth, "Effects of laser-modulated particulate incandescence on Raman scattering diagnostics," *J. App. Phys.* **48**, 4473–4479 (1977).
4. L. A. Melton, "Soot diagnostics based on laser heating," *Appl Opt.* **23**, 2201–2208 (1984).
5. C. J. Dasch, "New soot diagnostics in flames based on laser vaporization of soot," in *20th Symposium (International) on Combustion* (Combustion Institute, 1984), pp. 1231–1237.
6. R. L. Vander Wal and K. A. Jensen, "Laser-induced incandescence: excitation intensity," *Appl Opt.* **37**, 1607–1616 (1998).
7. R. L. Vander Wal, and D. L. Dietrich, "Laser-induced incandescence applied to droplet combustion," *Appl. Opt.* **34**, 1103–1107 (1995).
8. R. T. Wainner, J. M. Seitzman, and S. R. Martin, "Soot measurements in a simulated engine exhaust using laser-induced incandescence," *AIAA J.* **37**, 738–743 (1999).
9. R. L. Wal, Z. Zhou, and M. Y. Choi, "Laser-induced incandescence calibration via gravimetric sampling," *Combust. Flame* **105**, 462–470 (1996).
10. C. R. Shaddix, J. E. Harrington, and K. C. Smyth, "Quantitative measurements of enhanced soot production in a flickering methane/air diffusion flame," *Combust. Flame* **99**, 723–732 (1994).
11. B. Quay, T.-W. Lee, T. Ni, and R. J. Santoro, "Spatially-resolved measurements of soot volume fraction using laser-induced incandescence," *Combust. Flame* **97**, 384–392 (1994).
12. T. Ni, J. A. Pinson, S. Gupta, and R. J. Santoro, "Two-dimensional imaging of soot volume fraction by the use of laser-induced incandescence," *Appl. Opt.* **34**, 7083–7091 (1995).
13. R. L. Vander Wal and K. J. Weiland, "Laser-induced incandescence: development and characterization towards a measurement of soot-volume fraction," *Appl. Phys. B* **59**, 445–452 (1994).
14. N. P. Tait and D. A. Greenhalgh, "PLIF imaging of fuel fraction in practical devices and LII imaging of soot," *Ber. Bunsenges. Phys. Chem.* 1993. **97**, 1619–1625 (1993).
15. R. Puri, T. F. Richardson, R. J. Santoro, and R. A. Dobbins, "Aerosol dynamic processes of soot aggregates in a laminar ethene diffusion flame," *Combust. Flame* **92**, 320–333 (1993).
16. P. E. Bengtsson and M. Alden, "Application of a pulsed laser for soot measurements in premixed flames," *Appl. Phys. B* **48**, 155–164 (1989).
17. D. L. Hofeldt, "Real-time soot concentration measurement technique for engine exhaust streams," in *International Congress and Exposition*, SAE 930079 (Society of Automotive Engineers, 1993).
18. S. Schraml, S. Will, and A. Leipertz, "Simultaneous measurements of soot mass concentration and primary particle size in the exhaust of a DI Diesel engine by time-resolved laser-induced incandescence (TIRE-LII)," SAE 1999-01-0146 (Society of Automotive Engineers, 1999).
19. D. R. Snelling, "Development and application of laser-induced incandescence (LII) as a diagnostic for soot particulate measurements," in *Advanced Non-Intrusive Instrumentation for Propulsion Engines AGARD Conference Proceedings* (AGARD, 1997), Vol. 598, pp. 23.21–23.29.
20. S. Will, S. Schraml and A. Leipertz, "Comprehensive two-dimensional soot diagnostics based on laser-induced incandescence (LII)," in *26th Symposium (International) on Combustion* (Combustion Institute, 1996, pp. 2277–2284).
21. P. O. Witze, S. Hochgreb, D. Kayes, H. A. Michelsen, and C. R. Shaddix, "Time-resolved laser-induced incandescence and laser elastic-scattering measurements in a propane diffusion flame," *Appl Opt.* **40**, 2443–2452 (2001).
22. R. L. Vander Wal, T. M. Ticich and A. B. Stephens, "Optical and microscopy investigations of soot structure alterations by laser-induced incandescence," *Appl. Phys. B* **67**, 115–123 (1998).
23. R. M. Pon and J. P. Hessler, "Spectral emissivity of tungsten: analytic expressions for the 340-nm to 2.6-micron spectral region," *Appl Opt.* **23**, 975–976 (1984).
24. R. Jullien, and R. Botet, *Aggregation and Fractal Aggregates* (World Scientific, 1987).
25. J. E. Martin and A. J. Hurd, "Scattering from fractals," *J. Appl. Cryst.* **20**, 61–78 (1987).
26. T. L. Farias, M. G. Carvalho, Ü. Ö Köylü, and G. M. Faeth, "A computational study of the absorption and scattering properties of soot," in *Combustion Institute / Eastern Section Fall Technical Meeting* (Combustion Institute, 1993), pp. 394–397.
27. T. L. Farias, M. G. Carvalho, U. O. Köylü, and G. M. Faeth, "Computational evaluation of approximate Rayleigh–Debye–Gans/fractal-aggregate theory for the absorption and scattering properties of soot," *J. Heat Transfer* **117**, 152–159 (1995).
28. M. F. Iskander, S. C. Olson, R. E. Benner, and D. Yoshida, "Optical scattering by metallic and carbon aerosols of high aspect ratio," *Appl Opt.* **25**, 2514–2520 (1986).
29. J. Nelson, "Test of a mean field theory for the optics of fractal clusters," *J. Mod. Opt.* **36**, 1031–1057 (1989).
30. E. M. Purcell and C. R. Pennypacker, "Scattering and absorption of light by nonspherical dielectric grains," *Astrophys. J.* **186**, 705–714 (1973).
31. U. O. Köylü and G. M. Faeth, "Structure of overfire soot in buoyant turbulent diffusion flames at long residence times," *Combust. Flame* **89**, 140–156 (1992).
32. Y. A. Levendis, K. R. Estrada, and H. C. Hottel, "Development of multicolour pyrometers to monitor the transient response of burning carbonaceous particle," *Rev. Sci. Instrum.* **63**, 3608–3622 (1992).
33. F. Liu, B. J. Stagg, D. R. Snelling, and G. J. Smallwood, "Effects of primary soot particle size distribution on the temperature of soot particles heated by a nanosecond pulsed laser in an atmospheric laminar diffusion flame" *Int. J. Heat Mass Transfer* (to be published).
34. G. J. Smallwood, D. R. Snelling, F. Liu, and Ö. L. Gülder, "Clouds over soot evaporation: errors in modeling laser-induced incandescence of soot," *J. Heat Transfer* **123**, 814–818 (2001).
35. D. R. Snelling, F. Liu, G. J. Smallwood, and Ö. L. Gülder, "Evaluation of the nanoscale heat and mass transfer model of the laser-induced incandescence: prediction of the excitation intensity," in *Thirty Fourth National Heat Transfer Conference* (American Society of Mechanical Engineers, 2000), paper NHTC2000-12132.
36. D. R. Snelling, F. Liu, G. J. Smallwood, and Ö. L. Gülder, "Determination of the soot absorption function and thermal accommodation coefficient using low-fluence LII in a laminar coflow ethylene diffusion flame," *Combust. Flame* **136**, 180–190 (2004).
37. D. R. Snelling, K. A. Thomson, G. J. Smallwood, and Ö. L. Gülder, "Two-dimensional imaging of soot volume fraction in laminar diffusion flames," *Appl Opt.* **38**, 2478–2485 (1999).
38. A. V. Filippov and D. E. Rosner, "Energy transfer between an aerosol particle and gas at high temperature ratios in the Knudsen transition regime," *Int. J. Heat Mass Transfer* **43**, 127–138 (2000).
39. F. Liu, G. J. Smallwood, and D. R. Snelling, "Effects of primary particle diameter and aggregate size distribution on the temperature of soot particles heated by pulsed lasers," *J. Quant. Spectrosc. Radiat. Transfer* **93**, 301–312 (2005).

40. K. Tian, F. Liu, K. A. Thomson, D. R. Snelling, G. J. Smallwood, and D. Wang, "Distribution of the number of primary particles of soot aggregates in a nonpremixed laminar flame," *Combust. Flame* **138**, 195–198 (2004).
41. C. M. Sorensen, "Light scattering by fractal aggregates: a review," *Aerosol Sci. Technol.* **35**, 648–687 (2000).
42. S. S. Krishnan, K. C. Lin, and G. M. Faeth, "Extinction and scattering properties of soot emitted from buoyant turbulent diffusion flames," *J. Heat Transfer* **123**, 331–339 (2001).
43. D. R. Snelling, K. A. Thomson, G. J. Smallwood, O. L. Gülder, E. J. Weckman, and R. A. Fraser, "Spectrally resolved measurement of flame radiation to determine soot temperature and concentration," *AIAA J.* **40**, 1789–1795 (2002).